ISAR Imaging using FFT with Polar Reformatting of Measured RCS

Ahmad Bilal*, Syed M. Hamza, Ziauddin Taj, Shuaib Salamat, Messam Abbas
Department of Avionics Engineering
Air University, PAC Campus
Kamra, Pakistan
*ahmadbilal@aerospace.pk

***Abstract*—Synthetic Aperture Radar uses radar movement for target identification and is commonly used in airborne radar systems for various applications such as oceanography, glaciology and military surveillance. On the contrary, for range-cross range profiling, Inverse Synthetic Aperture Radar exploits the target motion and is employed in ground based radar systems. In this work, ISAR imaging of two stealth fighter aircraft models is performed by reformatting the scattered field data from a polar grid to a Cartesian grid using the nearest neighbor interpolation method. Although numerical noise generated by this interpolation is unavoidable, a comparison of experimental and simulation results shows that this method can be used for identification of major scattering centers on low observable targets.**

Keywords—Radar Cross Section; Anechoic Chamber; Inverse Synthetic Aperture Radar; Radar Imaging

I. INTRODUCTION

For military applications, identification of enemy aircrafts has always been a challenging problem. Previously, the phenomenon of resonance has been exploited for target identification [1-3] but this approach did not give reliable estimates because it depended on the aspect angle of the target and in addition, the echo was immersed in noise and clutter. A relatively modern and well established method, knows as Synthetic Aperture Radar (SAR), is a radar technique used by radar systems mounted on moving platforms such as aircrafts or satellites for terrain mapping or subsurface imaging [4-7]. It uses the motion of a radar antenna to emulate a greater aperture size than the physical aperture and applies coherent integration to improve the signal to noise ratio (SNR), hence, producing high resolution range-cross range profiles of the target [8]. The distance travelled by the aircraft during the interval in which the target echo returns is directly proportional to the incremented aperture size. It can be inferred from this statement that distant targets will produce larger synthetic apertures. The same technique is applied to immovable radar systems by exploiting the motion of the target instead of that of the radar system and is referred to as Inverse Synthetic Aperture Radar (ISAR) [9]. This technique exposes the scattering centers of a target and can be used to localize the positions on an aircraft model where radar absorbing materials should be applied to minimize its radar signature.

Since the target could be represented by any type of swerling models [10], for each frequency, all scattering centers produce different phases and hence, ISAR imaging relies on the received phase whose calculation and measurement accuracy defines the quality of the image [9,11]. Once the complex electric fields are computed, they should be transformed from frequency domain to spatial domain for localization of the scattering centers. To carry out this transformation, various spectrum estimation techniques including parametric and non-parametric methods have been proposed, each having its own advantages and disadvantages in terms of resolution and computation time [12,13]. While spectrum estimation techniques such as autoregressive (AR) model and Multiple Signal Classification algorithms are used for high resolution [14], FFT based methods, which are non-parametric, are preferred because they give sufficient resolution in relatively less computation time [9,13].

Depending on the required resolution and aspect and frequency sampling rates of the scattered field, ISAR imaging algorithms are broadly classified into two categories referred to as the Small Bandwidth, Small Angle method (SBSA) and Wide Bandwidth, Large Angles (WBLA) method [9]. SBSA method is used where radar bandwidth is small and low cross-range resolution is required. On the other hand, if high resolution is required such as in sub-surface imaging or enemy aircraft identification, WBLA method should be used. Although a computationally intensive direct integration method exists [9], WBLA method cannot be directly applied to the sampled fields because the collected data comes from a polar grid and small angle approximation does not hold for large angles.

While recent works in this domain focus on image resolution using compressed sensing [15,16] and neural networks [17,18], in this research, we have used an FFT based algorithm with polar, frequency domain Radar Cross Section (RCS) data collected over a wide bandwidth and large angles. The data are reformatted into a Cartesian grid and are transformed into the spatial domain ISAR image of the scattering target. We have repeated this procedure for two very detailed aircraft models and our key contribution lies in the fact that, in addition to the simulated RCS, for the sake of comparison, we have used RCS measurements carried out in an anechoic chamber which are rarely reported because of their cost and experimental complexities.

The organization of this work is given here. Section II outlines the mathematical background of our work while section III presents a comparison of the measured and computed RCS and ISAR images for two aircraft models. Section IV includes some future directions of this research and concludes this article.

II. Mathematical Model

The treatment of WBLA data is different as compared to SBSA because of the small angle and plane-wave assumptions in the latter case. For a 2D image, a double integral given in (1) is carried out either by numerical techniques, such as Simpson's integration rule, or by DFT.

$$PI(x,y) = \frac{1}{BW_k \Omega} \int_{\emptyset_1}^{\emptyset_2} \int_{k_1}^{k_2} E_s(k,\emptyset) \cdot e^{2j(kCos\emptyset x + kSin\emptyset y)} dk \cdot d\emptyset \quad (1)$$

Where,

$PI(x,y)$ =Profile Intensity

$E_s(k,\emptyset)$ =Scattered E-field as a function of spatial frequency and angle of incidence

BW_k = Bandwidth of wavenumber

Ω = Bandwidth of angles of incidence

To carry out this integral using numerical techniques, reformatting of the fields is not required since this integral covers all the points in $k-\emptyset$ space. However, because of the wide range of integration limits, it is not desirable in those systems where computational resources are limited or real-time imaging is required.

In order to use DFT, consider (2) that shows the E-field scattered from a point scatterer at (x_0, y_0).

$$E_s(k,\emptyset) \cong A \cdot e^{-2j(kCos\emptyset x_0 + kSin\emptyset y_0)} \quad (2)$$

The total scattered field (3) from a target is the sum of all the contributions from N scattering centers.

$$E_s^T(k,\emptyset) = \sum_{i=1}^{N} A_i \cdot e^{-2j(kCos\emptyset x_i + kSin\emptyset y_i)} \quad (3)$$

Since, $k_x = kCos\emptyset$ and $k_y = kSin\emptyset$, from the basic fourier transform equaiton, it is clear that there exists a fourier relationship between k_x and x and between k_y and y. All that is needed to be done is the mapping of data on the k_x-k_y grid as shown is Fig. 1. If the datum on polar grid lies between the points $(n \cdot \Delta k_x, (n+1) \cdot \Delta k_x)$ and $(m \cdot \Delta k_y, (m+1) \cdot \Delta k_y)$, it should be projected onto these points. To accomplish this, we use the nearest neighbour interpolation method which updates the four nearest neighbouring points on the k_x-k_y grid according to the following rule:

$$\widetilde{E_s}[n \cdot \Delta k_x, m \cdot \Delta k_y] = A_i \cdot \frac{R}{l_1} \quad (4)$$

$$\widetilde{E_s}[(n+1) \cdot \Delta k_x, m \cdot \Delta k_y] = A_i \cdot \frac{R}{l_2} \quad (5)$$

$$\widetilde{E_s}[(n+1) \cdot \Delta k_x, (m+1) \cdot \Delta k_y] = A_i \cdot \frac{R}{l_3} \quad (6)$$

$$\widetilde{E_s}[n \cdot \Delta k_x, (m+1) \cdot \Delta k_y] = A_i \cdot \frac{R}{l_4} \quad (7)$$

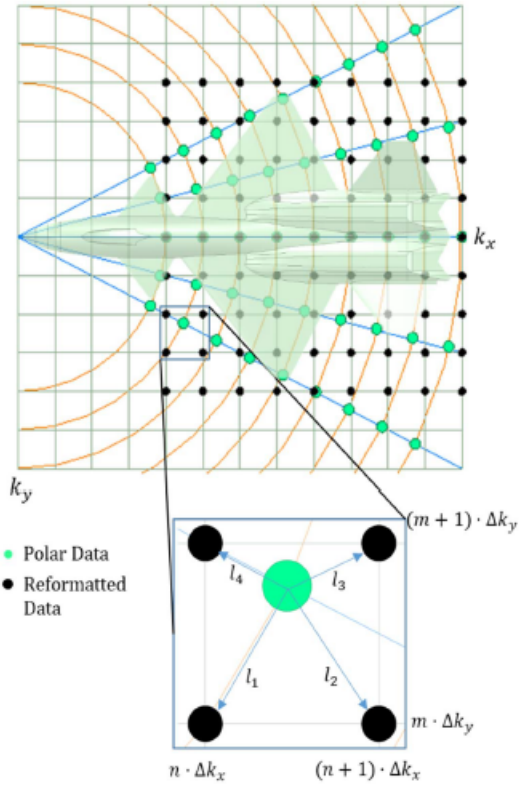

Figure 1: Polar reformatting of scattered fields onto k_x-k_y grid using nearest neighbour interpolation method

Where,

$$R = \frac{1}{\frac{1}{l_1} + \frac{1}{l_2} + \frac{1}{l_3} + \frac{1}{l_4}} \quad (8)$$

Once the interpolated fields are mapped onto the k_x-k_y plane, as shown in Fig. 1, a discrete, uniformly spaced grid is formed which is then fed to FFT for transformation to range-cross range profile of the target. The noise generated by this interpolation is unavoidable but it can be minimized by forming a closely spaced k_x-k_y grid which requires minimum possible values of Δk_x and Δk_y which eventually depends on the step size of the frequency and aspect angles. Hence, a smaller step in frequency and aspect angle produces images with better resolution and less interpolation noise. In addition, more neighboring points could also be used for a better approximation but it would add to the complexity of this algorithm.

III. Results

To validate this methodology, ISAR images were constructed using the complex monostatic RCS of two generic fighter aircraft models. This section shows the comparison between measured and computed RCS and between ISAR images constructed using these RCS values.

A. RCS Comparison

The two fighter aircraft models that were chosen for this research represent a generic configuration popular among the aircraft and radar designers. RCS was computed using the method of Shooting and Bouncing Rays (SBR) which is an asymptotic approach commonly used in place of computationally intensive Method of Moments (MoM). The effects of edge diffraction were taken into account using the Physical Theory of Diffraction and Uniform Theory of Diffraction [19].

For RCS measurements, two scaled down aircraft models were fabricated with a scaling factor of 1:8 and the measurement frequency in the anechoic chamber was scaled up by the same factor. Fig. 2 shows the RCS in dBm^2 at 1GHz frequency and VV polarization for both aircraft models. Table 1 shows the comparison in numeric form.

B. ISAR Images

To construct the ISAR images, a bandwidth of 2GHz was used for Model 1 with a center frequency of 1GHz. For Model 2, a bandwidth of 1.65GHz was used and center frequency was kept to be 800MHz. This requirement was necessitated because the scaling factors of both aircraft models were slightly different owing to their actual size. Complex monostatic RCS was computed and measured in azimuth plane for [0-2π] with a step size of 1°. Fig. 3 shows the images for both aircraft models computed using experimental and simulated data.

The noise in Fig. 3a and Fig. 3c can be attributed to the limited bandwidth and the applied interpolation which is still less than that of Fig. 3b and Fig. 3d which, in addition to the above mentioned sources, comes from the phase measurement imperfections. Further, model fabrication and the application of non-ideal conductive coating should also have played their role but it can be safely concluded that the simulated and measured ISAR images are in good agreement.

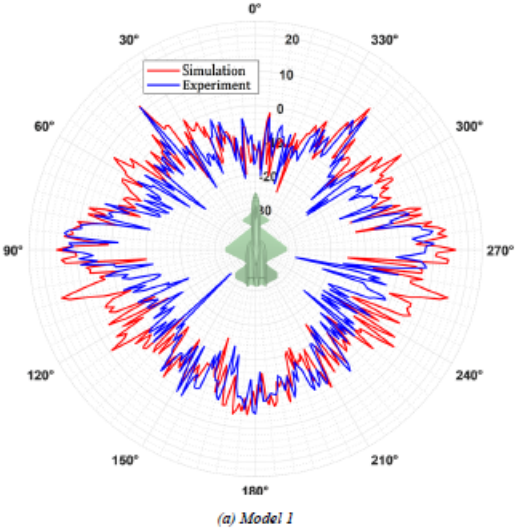

(a) Model 1

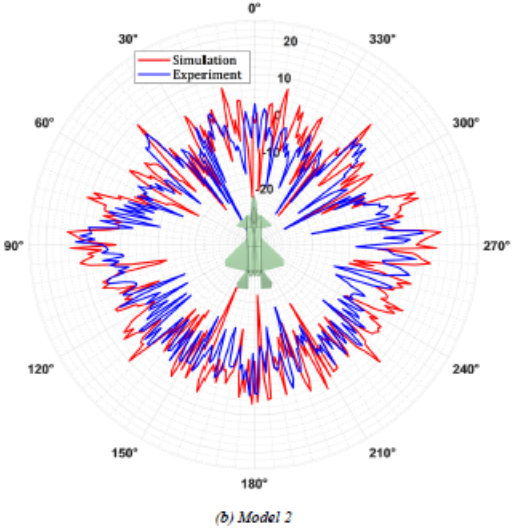

(b) Model 2

Figure 3: Measured and Simulated RCS of both aircraft models at 1 GHz VV Polarization using SBR Method

Table 1: All aspect RCS comparison of both aircraft models

Sector	Span (degrees)	Model 1 RCS (m^2)			Model 2 RCS (m^2)		
		Experimental	Simulation	Absolute Difference	Experimental	Simulation	Absolute Difference
Front	0°±45°	0.38	0.59	0.21	0.34	0.71	0.37
Rear	±180°±45°	0.7	0.7	0.01	0.57	0.97	0.4
Sideways	±90°±45°	1.33	3.9	2.58	1.06	2.5	1.43
Complete	0°±180°	0.94	2.25	1.3	0.76	1.66	0.9

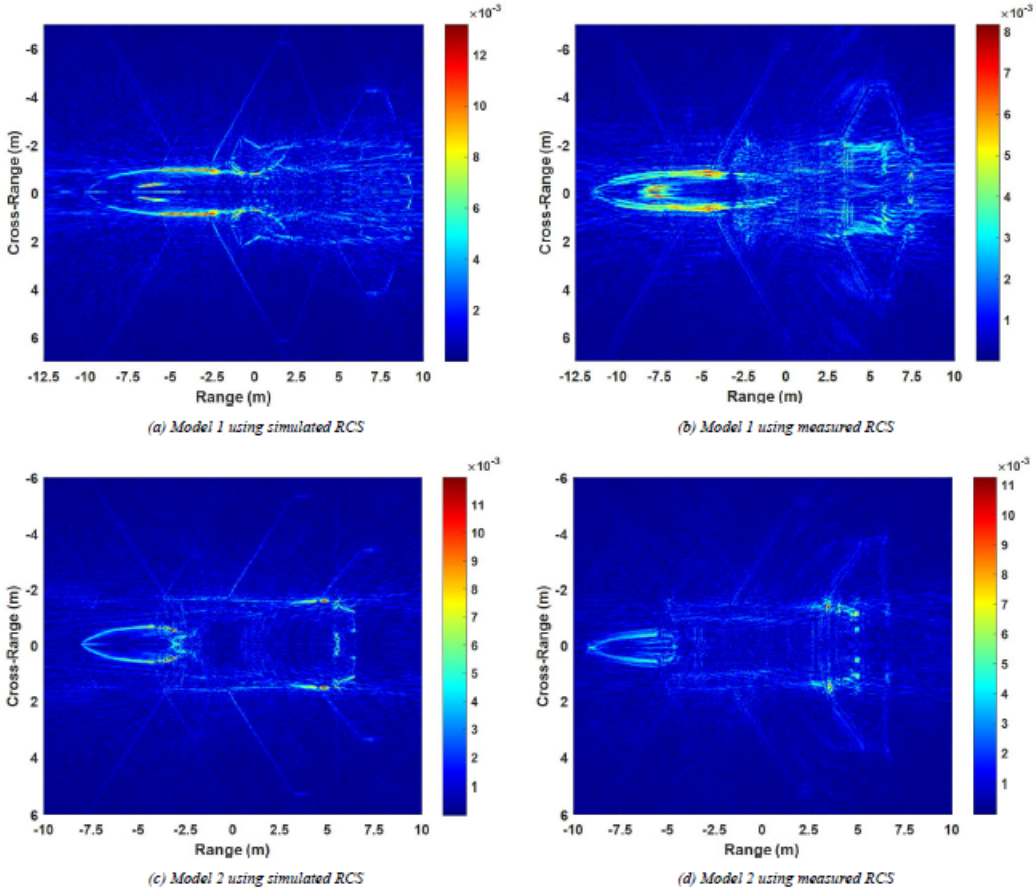

(a) Model 1 using simulated RCS

(b) Model 1 using measured RCS

(c) Model 2 using simulated RCS

(d) Model 2 using measured RCS

Figure 4:ISAR Images of both aircraft models using measured and simulated monostatic RCS in VV Polarization

IV. Conclusion and Future Directions

In this article, ISAR imaging using FFT of interpolated monostatic RCS in VV polarization is analyzed. Despite of the approximations of SBR and nearest neighbor interpolation method, a comparison of measured and simulated RCS and ISAR images shows great agreement. Hence, ISAR imaging can be used as a target identification method because of the involved integration process that improves the SNR. With polar reformatting, it can be used to quickly analyze the scattering centers of a target which can prove beneficial in RCS minimization by structural modifications and application of radar absorbing materials. To improve resolution and to reduce image noise, other interpolation methods and hybrid transformation algorithms should be tested which might highlight more hot-spots on the target.

References

[1] Rothwell, Edward, et al. "Radar target discrimination using the extinction-pulse technique." *IEEE Transactions on Antennas and Propagation* 33.9 (1985): 929-937.

[2] Chen, Kun-Mu, et al. "Radar target discrimination by convolution of radar return with extinction-pulses and single-mode extraction signals." *IEEE Transactions on Antennas and Propagation* 34.7 (1986): 896-904.

[3] Toribio, R., J. Saillard, and P. Pouliguen. "Identification of radar targets in resonance zone: E-pulse techniques." *Progress in electromagnetics Research* 43 (2003): 39-58.

[4] Griffiths, H. D., Christopher Baker, and David Adamy. *Stimson's introduction to airborne radar*. Scitech Pub Incorporated, 2014.

[5] Elsherbini, Adel, and Kamal Sarabandi. "Mapping of sand layer thickness in deserts using SAR interferometry." *IEEE Transactions on Geoscience and Remote Sensing* 48.9 (2010): 3550-3559.

[6] Hong, Seunghwan, et al. "Water area extraction using RADARSAT SAR imagery combined with landsat imagery and terrain information." *Sensors* 15.3 (2015): 6652-6667.

[7] Stefanik, Kevin V., et al. "UAV-based stereo vision for rapid aerial terrain mapping." *GIScience & Remote Sensing* 48.1 (2011): 24-49.

[8] Gorham, LeRoy A., and Linda J. Moore. "SAR image formation toolbox for MATLAB." *Algorithms for Synthetic Aperture Radar Imagery XVII*. Vol. 7699. International Society for Optics and Photonics, 2010.

[9] Ozdemir, Caner. *Inverse synthetic aperture radar imaging with MATLAB algorithms*. Vol. 210. John Wiley & Sons, 2012.

[10] Song, Xiufeng, et al. "Dominant-plus-Rayleigh models for RCS: Swerling III/IV versus Rician." *IEEE Transactions on Aerospace and Electronic Systems* 49.3 (2013): 2058-2064.

[11] Scheer, Jim, and William A. Holm. *Principles of modern radar*. Eds. Mark A. Richards, and William L. Melvin. SciTech Pub., 2010.

[12] Zhang, Siqian, Yutao Zhu, and Gangyao Kuang. "Imaging of downward-looking linear array three-dimensional SAR based on FFT-MUSIC." *IEEE Geoscience and Remote Sensing Letters* 12.4 (2014): 885-889.

[13] Park, Jong-Il, and Kyung-Tae Kim. "A comparative study on ISAR imaging algorithms for radar target identification." *Progress In Electromagnetics Research* 108 (2010): 155-175.

[14] Scharf, Louis L. *Statistical signal processing*. Vol. 98. Reading, MA: Addison-Wesley, 1991.

[15] Yang, Jungang, et al. "Compressed Sensing Radar Imaging: Fundamentals, Challenges, and Advances." *Sensors* 19.14 (2019): 3100.

[16] Massa, Andrea, Paolo Rocca, and Giacomo Oliveri. "Compressive sensing as a new paradigm in wave scattering and propagation." *2016 IEEE International Symposium on Antennas and Propagation (APSURSI)*. IEEE, 2016.

[17] Hu, ChangYu, et al. "Inverse synthetic aperture radar imaging using complex-value deep neural network." *The Journal of Engineering* 2019.20 (2019): 7096-7099.

[18] Hu, Changyu, et al. "Inverse Synthetic Aperture Radar Imaging Using a Fully Convolutional Neural Network." *IEEE Geoscience and Remote Sensing Letters* (2019).

[19] D. A. Mc Namara, C. W. I. Pistorius, and J. A. G. Malherbe.: 'Introduction to the Uniform Theory of Diffraction', (Artech House, 1990)